COMPARISON OF THERMAL AND OPTICAL BEHAVIORS OF PRE-MOLDED AND CERAMIC PACKAGE LIGHT EMITTING DIODES

LEE ZHI YIN

UNIVERSITI SAINS MALAYSIA
2013

COMPARISON OF THERMAL AND OPTICAL BEHAVIORS OF PRE-MOLDED AND CERAMIC PACKAGE LIGHT EMITTING DIODES

by

LEE ZHI YIN

Thesis submitted in fulfillment of the requirements
for the degree of
Master of Science

July 2013

ACKNOWLEDGEMENTS

First and foremost, I would like to send my gratitude to my project supervisor Assoc. Prof. Dr. Mutharasu Devarajan as well as my industrial supervisor Mr. Shahrol Izzanni who gave me the opportunity to study the project on the topic: Comparison of thermal and optical behaviors of pre-molded and ceramic package light emitting diodes. By this, I was provided a chance to participate in the development of light-emitting diode technology and the future challenges. With their excellent guidance and supports, I am able to conclude this project successfully.

Secondly, I am grateful to Mr. Luruthudass Annaniah and the engineers Ms. Gwynett Lee and Mr. Ng Kok Eng from the research and development department of OSRAM Opto Semiconductors (M) Sdn. Bhd. who are being patient for my doubts regarding to the technology. They are willing to spend their valuable time in conducting a group discussion for the purpose of knowledge sharing. Ms. Gwynett has even prepared a few Microsoft power point presentation slides on the fundamentals for my easy understanding and this has allowed me to gain much info in the shortest time. It is also important to acknowledge the technicians Mr. Fakhir, Mr. Kabil and Ms. Mardiana in providing the technical helps especially in the reflow soldering process and pole connection. With this, I have indirectly saved a lot of time from the long waiting list for the process.

Furthermore, I am thankful to the staffs from Nano-Optoelectronics Research and Technology Laboratory of Universiti Sains Malaysia for offering me the technical supports in the operation of the characterization systems.

Special thanks go to my seniors Ms. Anithambigai Permal and Ms. Teeba Nadarajan who had always rectified my mistakes, generous in sharing information and constructive suggestions. In addition, I would like to thank Ms. Lee Sze Yen for her day and night accompanies during the data collection; and Ms. Ching Chin Peng for her inspiring discussions. Not to forget my fellow lab-mates who have made a good collaboration throughout the project. Their contribution has brought to a successful completion of my project.

Besides, I wish to acknowledge MyBrain15 which established by Ministry of Higher Education, Malaysia in supporting my tuition fees. I intend to express my appreciation to Postgraduate Research Grant No. 1001/PFIZIK/834112 and Graduate Assistance Scheme by Universiti Sains Malaysia as well in providing the financial aid. Thus, I am able to purchase the needed resources without struggling for the payment.

I am blessed to have an amazing group of friends who always listened to my complaints, shared every moment of my happiness and sadness. Finally, I am most indebted to my family. Thanks for their consideration on my decision to further Master degree and always stand by me with unlimited love. Their encouragement has provided me the courage to face the challenges on my learning path.

TABLE OF CONTENTS

Page

ACKNOWLEDGEMENTS ……………………………………………………... ii

TABLE OF CONTENTS ……………………………………………………... iv

LIST OF TABLES ……………………………………………………… vii

LIST OF FIGURES ……………………………………………………... viii

LIST OF SYMBOLS ……………………………………………………… xiii

LIST OF ABBREVIATIONS ……………………………………………… xvi

ABSTRAK ………………………………………………………………... xvii

ABSTRACT ……………………………………………………………… xviii

CHAPTER 1: INTRODUCTION

1.1 Overview ……………………………………………………………... 1

1.2 Problems statement ……………………………………………………... 4

1.3 Objectives …………………………………………………………….. 5

1.4 Research contributions ……………………………………………….. 5

1.5 Organization of thesis ………………………………………………... 6

CHAPTER 2: LITERATURE REVIEW

2.1 Overview ……………………………………………………………... 7

2.2 Study on thermal and optical properties of LED …………………….. 7

2.3 Package thermal structure ……………………………………………. 8

2.4 Modification on board-level and system-level ……………………….. 13

2.5 Die-attach and thermal interface material ……………………………. 16

2.6 Improvement of thermal management ……………………………….. 18

2.7 Summary …………………………………………………………… 21

CHAPTER 3: METHODOLOGY AND INSTRUMENTATION

3.1 Overview ………………………………………………………….... 22

3.2 Experimental works

  3.2.1 Reflow soldering process and pole connection ………………. 22

  3.2.2 LED calibration ………………………………………………. 24

  3.2.3 Study on thermal and optical performances of LED …………. 26

  3.2.4 Application of external heat sink …………………………….. 29

  3.2.5 Effect of thermal interface material ………………………….. 29

  3.2.6 Thermal study of various end surface convections in different air environments ……………………………………………… 31

  3.2.7 Accuracy of thermal characterization

    3.2.7.1 Effective and real thermal resistances ……………… 33

    3.2.7.2 Driving current modes ……………………………... 36

3.3 Characterization systems

  3.3.1 Thermal transient tester (T3Ster) and T3Ster-Master software ……………………………………………………. 38

  3.3.2 Thermal and radiometric characterization of LEDs (TERALED) and Teraled-View software ……………………. 41

  3.3.3 Thermal imaging camera (TIC) and supporting software ……. 42

3.4 Summary ……………………………………………………....... 42

CHAPTER 4: RESULTS AND DISCUSSION

4.1 Overview ………………………………………………………….... 44

4.2 Relationship between thermal and optical performances of LED …… 44

4.3 Effects of contacting surface area and application of external heat sink ……………………………………………………………………… 52

4.4 Applications of thermal tape and thermal compound ………………... 57

4.5 Influences of natural and forced convections in open-air and still-air environments ………………………………………………………… 61

4.6 Accuracy of thermal transient recording

4.6.1 Distinction of effective and real thermal resistances ………… 69

4.6.2 Operating of LED with direct current and single-pulse mode … 72

4.7 Summary ………………………………………………………….... 77

CHAPTER 5: CONCLUSION

5.1 Conclusion ……………………………………………………….... 79

5.2 Recommendation for future research ………………………………… 81

REFERENCES ……………………………………………………………… 82

APPENDICES

APPENDIX 1: LEDs preliminary data

APPENDIX 2: Simultaneous recording of thermal and optical parameters

APPENDIX 3: Corresponding of electrical, optical and heat dissipation power to driving current

APPENDIX 4: Differential structure functions

LIST OF PUBLICATION

LIST OF TABLES

Page

Table 3.1: The notations for various measuring conditions. 34

Table 4.1: Thermal parameters for pre-molded and ceramic package LEDs. 53

Table 4.2: Ratio of the contacting surface area between the package-level LED and MCB. 54

Table 4.3: Thermal parameters for pre-molded and ceramic package LEDs with the presence of external heat sink. 56

Table 4.4: Ratio of the contacting surface area between the MCB and heat sink 57

Table 4.5: Junction-to-ambient thermal resistance for pre-molded package LED under various measuring conditions in open-air environment. 63

Table 4.6: Junction temperature and rate of heat dissipation for pre-molded package conducted under the selected conditions in open-air environment. 65

Table 4.7: Junction-to-ambient thermal resistance for pre-molded package LED under various measuring conditions in still-air environment. 66

Table 4.8: Junction temperature and rate of heat dissipation for pre-molded package LED that was conducted under the selected conditions in still-air environment. 68

Table 4.9: Thermal parameters of pre-molded package LED that was operated with driving current at 350mA and 700mA. 70

Table 4.10: Optical parameters of pre-molded package LED that was operated with driving current at 350mA and 700mA. 70

Table 4.11: Partial thermal resistances of the LED that was operated with different driving current modes. 74

Table 4.12: Junction-to-ambient thermal resistance, junction temperature and input power of the LED that was operated with different driving current modes. 74

LIST OF FIGURES

		Page
Figure 1.1:	Schematic diagram of GaN-based LED.	2
Figure 1.2:	CIE chromaticity diagram.	3
Figure 1.3:	Schematic diagram of lambertian reflector.	4
Figure 2.1(a):	Package thermal structure with cylindrical-shape heat slug.	9
Figure 2.1(b):	Package thermal structure with hexahedron-shape heat slug.	9
Figure 2.1(c):	Package thermal structure with Cu-thin-film coated package heat slug.	9
Figure 2.2(a):	The stress distributions for ceramic molds in the chip.	11
Figure 2.2(b):	The stress distributions for ceramic molds in the die attach.	11
Figure 2.3(a):	The stress distributions for plastic mold in the chip.	11
Figure 2.3(b):	The stress distributions for plastic mold in the die attach.	11
Figure 2.4(a):	Simulation result of temperature distribution for Package **A**.	12
Figure 2.4(b):	Simulation result of temperature distribution for Package **B**.	12
Figure 2.5:	Thermal transients for Types **I** and **II**.	13
Figure 2.6:	Thermal transient and simulation result for Type **III**.	13
Figure 2.7:	Schematic diagram of MCB.	14
Figure 2.8(a):	Schematic diagram of the main flow for the pins in vertical up-facing.	15
Figure 2.8(b):	Schematic diagram of the main flow for the pins in sideward-facing.	15
Figure 2.8(c):	Schematic diagram of the main flow for the pins in vertical down-facing.	15

Figure 2.9: Schematic diagram of the heat sink geometry. 15

Figure 2.10(a): The interfaces of before the application of thermal interface material. 16

Figure 2.10(b): The interfaces of after the application of thermal interface material. 16

Figure 2.11(a): Thermal impedance in a function of time with thermal grease 17

Figure 2.11(b): Thermal impedance in a function of time without thermal grease. 17

Figure 2.12: Mechanism of thermo-electric cooling. 18

Figure 2.13: The temperature variations of the LED substrate and cooling fins at 9W. 19

Figure 2.14: Schematic diagram of piezoelectric fan. 19

Figure 2.15: The compact cooling module. 20

Figure 2.16: Basic setup of microjet cooling system for high power LEDs. 21

Figure 3.1(a): Schematic diagram of pre-molded package LED. 23

Figure 3.1(b): Schematic diagram of ceramic package LED. 23

Figure 3.2: Reflow soldering profile for pre-molded and ceramic package LEDs. 24

Figure 3.3: Flowchart of the procedures for reflow soldering and pole connection. 25

Figure 3.4: Flowchart of the LED calibration process. 27

Figure 3.5: Flowchart of thermal and optical characterizations for pre-molded and ceramic package LEDs. 28

Figure 3.6: Flowchart of thermal characterization of the LEDs with the application of an external heat sink. 30

Figure 3.7(a): Schematic diagrams of **S1** attached to an external heat sink with thermal tape (**ST**). 31

Figure 3.7(b): Schematic diagrams of **S1** attached to an external heat sink with thermal compound (**SP**). 31

Figure 3.8: Flowchart of the thermal characterization on pre-molded package LED under the influence of different thermal interface materials. 32

Figure 3.9 (a): The measurement setup for thermal characterization on pre-molded package LED in an open-air environment. 33

Figure 3.9(b): The measurement setup for thermal characterization on pre-molded package LED in still-air environment. 33

Figure 3.10: Flowchart of thermal characterization on pre-molded package LED in various measuring conditions. 34

Figure 3.11: Flowchart of simultaneous thermal and optical characterizations on pre-molded package LED. 35

Figure 3.12(a): The flow of direct current at ***I*** (mA). 36

Figure 3.12(b): The flow of pulse current at ***I*** (mA). 36

Figure 3.13: Thermal transient measurement profile. 36

Figure 3.14: Flowchart of thermal characterization on pre-molded package LED. 37

Figure 3.15: Time-constant spectrum of an identical device with Foster equivalent. 38

Figure 3.16: Package-level LED mounted on an MCB and attached to heat sink. 39

Figure 3.17: Representation of an LED in forms of Cauer equivalent. 39

Figure 3.18(a): Cumulative structure function for an identical device. 40

Figure 3.18(b): Differential structure function for an identical device. 40

Figure 3.19: Schematic diagram of the operation of Thermal and Radiometric Characterization of LEDs. 41

Figure 3.20: Reflect, absorb and transmit of infrared energy. 42

Figure 4.1: Graph of luminous intensity versus driving current for pre-molded and ceramic package LEDs. 45

Figure 4.2: Graph of efficiency versus driving current for pre-molded and ceramic package LEDs. 46

Figure 4.3: Graph of junction temperature versus driving current for pre-molded and ceramic package LEDs. 46

Figure 4.4: Graph of efficiency versus junction temperature for pre-molded package LED. 47

Figure 4.5: Cumulative structure functions of pre-molded package LED at increasing driving current. 49

Figure 4.6: Cumulative structure functions of ceramic package LED at increasing driving current. 49

Figure 4.7(a): Schematic diagram of pre-molded package LED mounted on MCB. 50

Figure 4.7(b): Schematic diagram of ceramic package LED mounted on MCB. 50

Figure 4.8: Graph of drop-voltage versus temperature for pre-molded and ceramic package LEDs. 52

Figure 4.9: Cumulative structure functions for pre-molded and ceramic package LEDs. 53

Figure 4.10: Schematic diagram shows the dependency of heat conduction of an LED on the surface area. 55

Figure 4.11: Cumulative structure functions for pre-molded and ceramic package LEDs with the presence of external heat sink. 55

Figure 4.12: Schematic diagram of heat sink for heat conduction and convection. 57

Figure 4.13: Graph of drop-voltage versus temperature for ceramic package LED. 58

Figure 4.14: Cumulative structure functions for ceramic package LED with conditions of **S1**, **ST** and **SP**. 58

Figure 4.15: Differential structure functions for ceramic package LED with conditions of **S1**, **ST** and **SP**. 59

Figure 4.16: Graph of drop-voltage versus temperature for pre-molded package LED. 61

Figure 4.17: Differential structure functions for pre-molded package LED under various measuring conditions in open-air environment. 62

Figure 4.18(a)(i): Thermal images for **p_off** with driving current of 150mA. 64

Figure 4.18(a)(ii): Thermal images for **p_off** with driving current of 700mA. 64

Figure 4.18(b)(i): Thermal images for **p_up** with driving current of 150mA. 64

Figure 4.18(b)(ii): Thermal images for **p_up** with driving current of 700mA. 64

Figure 4.18(c)(i): Thermal images for **p_down** with driving current of 150mA. 64

Figure 4.18(c)(ii): Thermal images for **p_down** with driving current of 700mA. 64

Figure 4.19: Differential structure functions for pre-molded package LED under various measuring conditions in still-air environment. 67

Figure 4.20: Differential structure functions for pre-molded package LED that was operated with biasing current of 350mA and 700mA. 69

Figure 4.21: Differential structure functions evaluated in term of real thermal resistance for pre-molded package LED under various influencing factors. 71

Figure 4.22: Graph of drop-voltage versus temperature. 72

Figure 4.23: Cumulative structure functions of the LED that was operated with different driving current modes. 73

Figure 4.24: Differential structure functions of the LED that was operated with different driving current modes. 73

Figure 4.25: Electrical disturbance in the recorded thermal transient for the LED that was operated with direct current at 30 minutes operating time. 76

Figure 4.26: Electrical disturbance in the recorded thermal transient for the LED that was operated with single-pulse mode at 30 minutes operating time. 76

LIST OF SYMBOLS

(x,y)	Chromaticity coordinates x and y
A	Ampere
A	Surface area
A_B	Surface area of base
A_c	Contact area
$A_{cross\text{-}section}$	Area of cross-section
$A_{heatflow}$	Heat flow area
A_{MCB}	Surface area of metal-core board
$A_{package}$	Surface area of package-level LED
A_T	Total surface area
C	Coulomb
C_{th}	Thermal capacitance
Hz	Hertz
I	Driving current
J	Current density
K	Kelvin
k	Thermal conductivity
m	Milli
mm	Millimeter
mm^2	Millimeter square
η	Efficiency
Ø	Luminous intensity
℃	Degree celsius

P_{el}	Electrical power
P_h	Heat dissipation power
P_{in}	Input power
P_{opt}	Optical power
q	Charge of an electron
Q	Rate of heat dissipation
R_{th}	Thermal resistance
R_{thBA}	Board-to-ambient thermal resistance
R_{thBH}	Board-to-heat sink thermal resistance
R_{thCB}	Case-to-board thermal resistance
R_{thDC}	Die-attach-to-case thermal resistance
R_{thHA}	Heat sink-to-ambient thermal resistance
R_{thJA}	Junction-to-ambient thermal resistance
R_{thJB}	Junction-to-board thermal resistance
R_{thJC}	Junction-to-case thermal resistance
R_{thJD}	Junction-to-die-attach thermal resistance
R_{thl}	Effective thermal resistance
R_{thr}	Real thermal resistance
s	Second
Σ	Summation
T	Temperature
t	Thickness
T_A	Ambient temperature
T_J	Junction temperature
T_o	Absolute temperature

V	Voltage
V_T	Thermal voltage
W	Watt
ΔT	Change in temperature
ΔV	Change in voltage
κ	Boltzmann constant
μm	Micrometer

ABBREVIATIONS

CCT	Color temperature
CIE	International Commission on Illumination
CTE	Coefficient of thermal expansion
et al.	Latin: et alii (and others)
FEA	Finite element analysis
FEM	Finite element method
FVM	Finite volume method
JEDEC	JEDEC Solid State Technology Association (Formerly: Joint Electron Engineering Council)
LED	Light-emitting diode
MBE	Molecular beam epitaxy
MCB	Metal-core board
MOCVD	Metal-organic chemical vapor deposition
PCB	Printed-circuit board
RGB	Red, green and blue
SEM	Scanning electron microscopy
SMT	Surface mount technology
T3Ster	Thermal transient tester
TEC	Thermo-electric
TERALED	Thermal and radiometric characterization of light emitting diode
TIC	Thermal imaging camera
TIM	Thermal interface material
TSP	Temperature-sensitive parameter

PERBANDINGAN CIRI-CIRI TERMA DAN OPTIK TERHADAP DIOD PEMANCAR CAHAYA PAKEJ PRA-ACUAN DAN SERAMIK

ABSTRAK

Projek ini mengenai pencirian terma dan optik ke atas diod pemancar cahaya (LED) pakej pra-acuan dan seramik yang telah dijalankan dengan teknik rakaman haba fana dan pancaran cahaya. Diperhatikan bahawa keamatan cahaya daripada LED bergantung kepada arus input. Disebaliknya, kecekapan LED untuk menghasilkan kuasa optik berkurangan sebanyak 15% dengan kenaikan arus input. Ini disebabkan kepadatan ketumpatan arus input dan pemanasan pada simpang LED. Analisis pada tahap pakej dan sistem LED pakej pra-acuan menunjukkan rintangan haba simpang-ke-selongsong dan simpang-ke-persekitaran yang 13% dan 15% lebih rendah daripada pakej seramik. Tetapi, pelesapan haba LED pakej seramik telah dipertingkatkan dengan penggunaan papan litar bercetak. Kesan bahan pembungkusan dan nisbah antara kawasan permukaan telah digunakan untuk menjelaskan kes tersebut. Seterusnya, kajian telah menunjukkan bahawa penggunaan terma sebatian sebagai bahan antara permukaan telah mencapai rintangan haba simpang-ke-persekitaran yang sebanyak 6% lebih rendah daripada terma pita. Seterusnya, di persekitaran udara terbuka, pelesapan haba bagi LED pakej pra-acuan yang berkesan tercapai dengan kipas penyejukan menghadap ke atas; manakala, di persekitaran udara tertutup, ini tercapai dengan kipas penyejukan menghadap ke bawah. Akhirnya, pertimbangan kuasa optik dalam penentuan rintangan haba sebenar dapat meningkatkan ketepatan rakaman fana haba. Secara berturutan, LED yang beroperasi dengan arus terus menunjukkan rakaman fana haba yang lebih tepat dan dipercayai, di mana kemunculan gangguan elektrik dapat dikurangkan.

COMPARISON OF THERMAL AND OPTICAL BEHAVIORS OF PRE-MOLDED AND CERAMIC PACKAGE LIGHT EMITTING DIODES

ABSTRACT

The project signifies thermal and optical characterizations of pre-molded and ceramic package light emitting diodes (LEDs) that are conducted by using thermal transient and light emission recording techniques. It was observed that the luminous intensity of the LEDs is dependent on the input current. However, the LEDs efficiency is reduced for about 15% with the current increases, which due to the high current density and heating of LED junction. In terms of package-level and system-level, pre-molded package LED shows approximately to 13% and 15% lower in junction-to-case and junction-to-ambient thermal resistances respectively than ceramic package LED. Despite, the heat dissipation of ceramic package LED is improved after mounting on a metal-core board (board-level). Here, the effects of packaging material properties and ratio of contacting surface area are applied. Next, the results shows that the application of thermal compound as thermal interface material yields about 6% lower junction-to-ambient thermal resistance than thermal tape. Further investigation shows that the optimum heat convection for pre-molded package LED in an open-air environment is obtained as the cooling fan facing upward; while in terms of still-air environment, it is achieved as the cooling fan facing downward. Lastly, the accuracy of the captured thermal transient is improved by considering the optical power into the determination of real thermal resistance. In sequence, it was seen that the use of direct current reveals more accurate and reliable measurement results where the occurrence of electrical disturbance is minimized.

CHAPTER 1

INTRODUCTION

1.1 Overview

Light emitting diode (LED) is an astonishing invention of solid-state lighting which has brought in a new revolution in the lighting market, where the first commercialized red emission LED was invented by Holonyak and Bevacqua (1962). LED is well known with its characteristics such as environmentally friendly, excellent color saturation and high brightness. In addition, the operating lifetime of an LED is up to 50,000 hours and requires low power consumption (Weng, 2009). Nowadays, LED has been widely used in streetlight, residential, decoration and targeted to replace the conventional incandescent lamp in the future.

The p-n junction of an LED that was designed to convert the electrical energy into the electromagnetic radiation is made of III-IV semiconductor material. Both the direct and indirect band gap semiconductors are commonly being utilized to fabricate the junction. There are several methods have been presented in order to deposit a uniform junction structure on a substrate. Two of the proposed modern techniques are metal-organic chemical vapor deposition (MOCVD) and molecular beam epitaxy (MBE) (Zhang, et al., 2009; Wakui, et al. 2009). Radiation of incoherent light is occurred during the radiative recombination process under forward-bias condition, where the electrons from the conduction band tend to recombine with the holes in the valence band (Schubert, 2002a). The schematic diagram of GaN-based LED is shown in Figure 1.1.

Today, the emission wavelength of an LED has been extended and covered between the deep ultraviolet and infrared region. The specific emission wavelength of an LED can be varied by changing the *x*-composition of a particular material, for example: aluminum gallium arsenide ($Al_xGa_{1-x}As$), indium gallium arsenide ($In_xGa_{1-x}N$) and gallium arsenide phosphide ($GaAs_{1-x}P_x$).

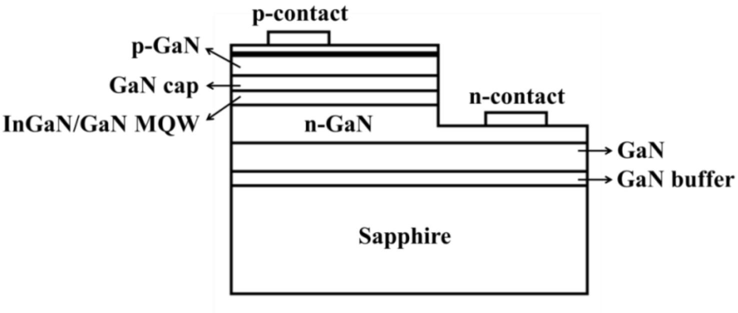

Figure 1.1: Schematic diagram of GaN-based LED. [Referred to Nguyen, 2010].

In order to produce an LED with white emission, phosphor-conversion and mixing of three-primary colors (*IESNA technical memorandum on light emitting diode (LED) sources and systems*, 2005) technologies have been proposed. In the phosphor-conversion technology, a blue-LED chip is covered with yellow phosphor. The blue light emitted from the chip is partly absorbed by the phosphor particles and yellow phosphorescence is reemitted (Chou, et al., 2005). Basically, the final emitted light depends on the scattering times which correspond to the thickness and concentration of the phosphor coating. Warm-white emission is produced as more scattering times and consists of longer propagation length, whereas ultra-white emission is produced as less scattering times and consists of shorter propagation length. However, the scattering enhancement particle such as silicon dioxide (SiO_2) has been suggested to be added into phosphor in order to obtain a uniform white emission (Liu, et al., 2009).

On the other hand, by combining the three-primary colors included red, green and blue (RGB), it is possible to generate any visible emission (Muthu, et al., 2002). The International Commission on Illumination (CIE) standard is a form of basis for most color measurement instruments (Stone and Bliss, 2005). The CIE chromaticity diagram, as shown in Figure 1.2, is the most common way of visualizing the chromaticity coordinates (x, y). The chromaticity coordinates can be expressed in terms of tristimulus values of X, Y and Z.

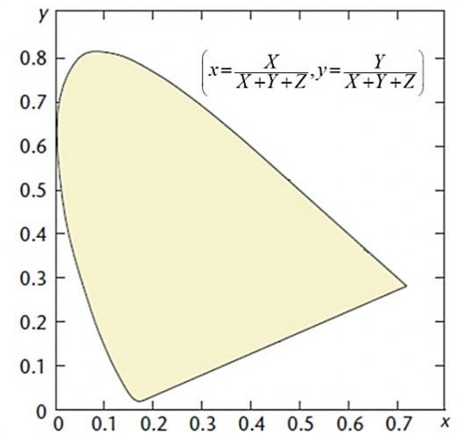

Figure 1.2: CIE chromaticity diagram. [Adapted from Stone and Bliss, 2005].

Besides, a “Brilliant Mix” concept has been proposed by Stich, et al. (2011) to generate white emission with high rendering index. The methodologies can be performed either by combining multiple colored semiconductor chips (usually RGB) in multi-packages or in LED cluster or by combining a semiconductor chip (blue) with a converter material in a single package. However, there are a few challenges such as decrease of operating temperature (T), controlling of color temperature (CCT) and luminous flux need to be confronted.

Mostly, LED sources are designed to have Lambertian beam distributions. According to Lambert’s cosine law, the source luminance is independent on the viewing angle (Pickover, 2008). In this case, to human eye, it shows the similar apparent radiance. Figure 1.3 shows the schematic diagram of a Lambertian reflector. It is assuming that a Lambertian source has an intensity of I along the direction at an angle of θ on a reflector surface with surface area of A, as written in equation 1.1.

$$I = I_n \cos\theta \tag{1.1}$$

where I_n indicates intensity emitted normal to the reflector surface.

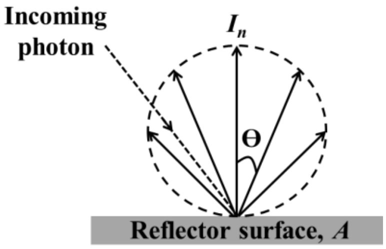

Figure 1.3: Schematic diagram of lambertian reflector. [Referred to Schubert, 2002b].

Here, luminance (L_v) which defined as intensity per unit area that was visible by an observer at a projected area, $A\cos\theta$ can be written as equation 1.2. As shown in equation 1.3, L_v is a constant, and thus, it is not being affected by viewing angle.

$$L_V = \frac{I_n A\cos\theta}{A\cos\theta} \tag{1.2}$$

$$L_V = I_n \tag{1.3}$$

There is a study showed that about 20% of the input power (P_{in}) is being converted into visible light and the rest is being transformed into heat (Cheng, et al., 2009). In this case, the poor thermal management of an LED will cause to the heat accumulation in the package. The continuous operating of an LED at an elevated T will accelerate its performance degradation and lead to device failure. Hence, the package thermal structure which constructed by using the packaging material with excellent thermal conductivity (k) (Liu and Luo, 2011) as well as low cost is desired as to enhance the capability of an LED to dissipate the heat generated to ambient.

1.2 Problems statement

Generally, there are two kinds of recombination processes, which are radiative and non-radiative recombination. In terms of radiative recombination, radiation with the energy equal to the band gap energy is emitted; whereas in terms of non-radiative recombination, the excess energy is emitted as heat. A study shows that approximately to 80% of P_{el} is being converted into P_h, thus the effectiveness of thermal structure of package LED in dissipating the heat generated has become a critical issue. Despite an LED exhibits the excellent optical properties, the inherently poor heat management may lead to LED degradation. Furthermore, the application of an LED with poor heat dissipation at a high operating T will enhance its failure rate where delamination and thermal stress between the material layers can be easily occurred. Here, pre-molded and ceramic package LEDs with similar active region size, but different package thermal structure is selected for investigation. The former is a widely used heat-slug-based LED with lower production cost, while the latter is an advance invention of ceramic-based LED which needs higher cost.

1.3 Objectives

The study on thermal and optical properties of an LED is important as to understand the uniqueness of LED operating properties. The main objectives of this work are listed as below:

a. To determine the relationship between thermal and optical behaviors of pre-molded and ceramic package LEDs.
b. To study the LED performances of pre-molded and ceramic packages under the influence of various measuring conditions.

1.4 Research contributions

The proposed work allows the study of thermal and optical properties of an LED to be performed through a simple yet detailed methodology. The outcome of this research would beneficial for LED manufacturing industrials as well as researchers in terms of providing the parties an understanding on the operating properties of the LEDs with different package thermal structures. Although thermal structure plays an important role in offering an effective heat path for heat dissipation of an LED, the equally important of end surface convection in influencing the rate of heat dissipation is described through the study. Besides, the work provides a reliable idea in selecting a suitable thermal interface material to be applied between the contacting surfaces as to obtain low thermal contact resistance. The last but not least, the improvement on the accuracy of thermal transient recording is revealed from the work.

1.5 Organization of thesis

In this thesis, there are five chapters to be presented. Generally, chapter one is about the introduction on the project. Brief descriptions were performed on the fundamental of an LED and the facing challenges in designing an effective package thermal structure. Besides, the aims to conduct the project and its contribution to the community are clearly identified.

This is followed by chapter two, where reviews on the theoretical, methodologies and substantive findings were showed. In subsequent, the proposed methodologies for this work are described in chapter three. Basically, the chapter is divided into two main parts, which highlight on the experimental works and introduction on the characterization systems.

Later, the obtained experimental results are presented and discussed in chapter four. Here, the comparison of thermal and optical performances between the LEDs is carried out as well as the determination of the influence of various measuring factors on the LEDs performance. Finally, conclusion on this project is written in chapter five. In addition, the recommendation for future studies as to improve the current methodology is included in the chapter.

CHAPTER 2

LITERATURE REVIEW

2.1 Overview

At the beginning of the chapter, reviews on theoretical and methodology for thermal and optical characterizations of LED are presented as well as the substantive findings from the researchers on the works. For the past few decades, thermal management of LED has become a critical challenge in order to maintain its performance and operating lifetime. Presently, a lot of efforts have been contributed by the researchers in improving the heat dissipation rate (Q) with the modification in package thermal structure, development of TIM, fluid and fan cooling methods. In addition, various characterization methods have been proposed to investigate the operating properties of an LED. In terms of real-time measurement, characterization system such as T3Ster has been commonly adopted; whereas in terms of simulation, finite element analysis (FEA) has been applied in the studies.

2.2 Study on thermal and optical properties of LED

Generally, T_J can be applied as LED performance indicator, where the light output of LED is dependent on its T_J (Poppe and Lasance, 2009). The operation of LED at an elevated T will lead to the performance degradation and shorten its lifespan. Basically, the conventional measuring method of T_J is performed by placing a high precision thermocouple wire close to the surface of an LED (*Package thermal characterizatio*n, 1999). However, the misplacement of thermocouple will cause to the determination of inaccurate T_J. As suggested by Lee and Park (2004), the nematic liquid crystal thermography measurement is another approximate approach to determine the surface temperature of an LED as T_J. With this, Szekely (1997) has proposed the measuring of thermal step-response function in determining the thermal performance of a semiconductor device, where the T-rise of a semiconductor device can be recorded over a wide range of time.

On the other hand, Farkas, et al. (2004) has presented an idea to investigate the thermal and optical performances of an LED simultaneously by utilizing the combined of Thermal Transient Tester (T3Ster), 3 inch integrating sphere and spectrometer. In this work, both the LED testing and simulation were carried out. The real-time measurement was carried out by capturing the light emitted from an LED and recording the thermal response function over a range of time, whereas SPICE-like circuit simulator was applied for LED simulation.

The experimental results revealed that η of light emission was slightly reduced (Narendran, et al., 2004), junction-to-ambient thermal resistance (R_{thJA}) was diminished (Farkas, et al., 2005) and T_J was enhanced with driving current (I) increases from 60mA, 75mA, 150mA and 300mA. In fact, the modeling outcomes showed that the energy transport of the LED was not accurately described through single R_{th} of either R_{thl} or R_{thr}. The authors have made a distinction between R_{thl} and R_{thr} to explain the thermal properties of a conventional device and an LED package, respectively. Besides, Narendran and Gu (2005) have carried out a lifetime test on a white-LED by varying the ambient temperature (T_A). The authors found that both the light output and lifespan of the LED were decreased at the increasing of T_A.

2.3 Package thermal structure

The package thermal structure of an LED plays an important role in providing an effective heat path for the heat conduction and convection processes from the LED junction to ambient. The most direct method for the improvement on thermal structure is by selecting high *k* packaging material such as the employment of heat slug, where the chip was attached to the slug by applying low R_{th} die-attach (Minges, 1989). However, a study has been carried out by Ra, et al. (2007) on four heat slugs with different geometrical structures. The structures were included cylindrical-shaped heat slug with expanded volume, cone-shaped heat slug with increased area, hexahedron-shaped heat slug and 20-μm Copper (Cu)-thin-film coated package on a printed-circuit board (*PCB*), as shown in Figure 2.1.

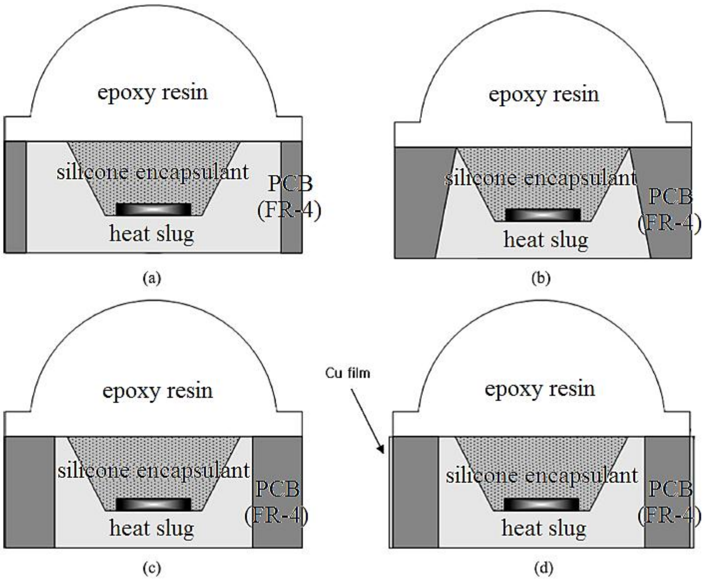
epoxy resin
silicone encapsulant
PCB
(FR-4)
heat slug
(a)
epoxy resin
silicone encapsulant
PCB
(FR-4)
heat slug
(b)
epoxy resin
silicone encapsulant
PCB
(FR-4)
heat slug
(c)
Cu film
epoxy resin
silicone encapsulant
PCB
(FR-4)
heat slug
(d)

Figure 2.1: Package thermal structure with: (a) cylindrical-shape, (b) cone-shape, (c) hexahedron-shape and (d) Cu-thin-film coated package heat slug. [Adapted from Ra, et al., 2007].

The chip was attached to the designed heat slug and *I* increases from 150mA to 300mA, in steps of 50mA was supplied to the LED. Basic knowledge of the electrical characteristic of LED has been applied to determine the voltage change (ΔV) in the measured T_J; whereas the finite volume method (FVM) has been used as a function of *I* and package structure for LED simulation. FVM or widely known as FEA or finite element method (FEM) is a sophisticated simulation software which applied in analyzing the solid mechanic, fluid flow, heat transfer, electric and magnetic fields. It utilized an extension of matrix method of structural analysis by dividing a target into small regions. Then, an approximately function and color representation were used to describe each of the particular regions (Bhavikati, 2005). The experimental and simulated results showed that T_J of the conditions was increased as I enhanced. However, the (d)-condition has demonstrated the most efficient heat transfer and lower thermal stress between the interfaces. This was because both the conduction and convection mechanisms were involved in the heat dissipation process, where more heat has been transferred to the ambient through Cu-film. Later, the utilization of leadframe in LED packaging has been adopted. Instead of the possibility in enhancing heat flow from the LED junction, the use of leadframe is capable in providing a mechanical support to the chip during assembly.

In the recent years, ceramic has become an alternative choice for LED packaging technology. Ceramic consists of high chemical stability which allows it to withstand hazardous environment. The other unique property of ceramic is the flexibility to form small and thin structure (Noor, et al., 1994). Although ceramic shows lower k due to the un-free movement of electrons, it consists of lower coefficient of thermal expansion (CTE) than metal which reduces the occurrence of lattice mismatch with the chip (Boch and Niepce, 2010). Hu, et al. (2007) has proposed the replacement of ceramic with plastic mold for LED packaging. In general, the model is composed by sapphire chip, heat slug, leadframe, ceramic mold and epoxy lens. Both the thermal transient recording and modeling have been carried out by using T3Ster and FEA simulation software, respectively. The cooling transient was recorded after the LED was switched-on at 350mA for 10 minutes; while simulation was performed to study the mechanical performance of the LED that was heated in an isothermal heat block at 270 ℃ for 20s. The findings showed that ceramic mold exhibited better thermal performance than plastic mold where higher T_J was observed in plastic than ceramic mold. Besides, the thermo-mechanical modeling revealed that lower stress has been created between the chip and die attach with ceramic molds. The stress distribution in the chip and die attachment for the ceramic mold is shown in Figures 2.2(a) and 2.2(b), while for the plastic mold was illustrated in Figures 2.3(a) and 2.3(b), respectively.

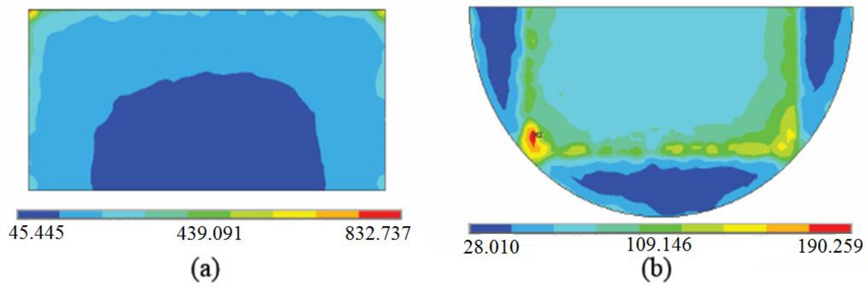

Figure 2.2: The stress distributions for ceramic molds: (a) in the chip and (b) in the die attach. [Adapted from Hu, et al., 2007].

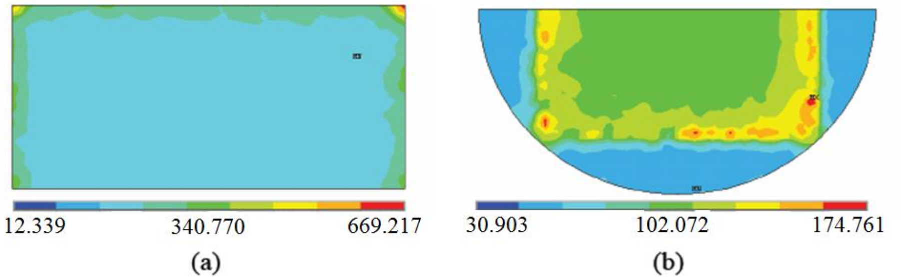

Figure 2.3: The stress distributions for plastic mold: (a) in the chip and (b) in the die attach. [Adapted from Hu, et al., 2007].

The existence of stress between the layers will lead to the problems such as breakage of wire bond, crack and delamination of the interface. Furthermore, ceramic has better moisture-proof ability than plastic. This is important in terms of eliminating the occurrence of moisture in the package which will reduce Q. In subsequence, Christensen and Graham (2009) have proposed an investigation on the thermal effect of high power LED packaging. Two types of high power LED packages with the die attached on metal-slug, named as Package **A** and another attached on ceramic sub-mount, named as Package **B** were adopted for the study.

The LEDs were then arranged in a square array on an aluminium (Al) core heat spreader. The temperature distribution of the system has been analyzed through FEA software. Figures 2.4(a) and 2.4(b) show the simulation results of temperature distribution for Package **A** and Package **B**, respectively. The results showed that Package **B** exhibited lower package R_{th} and higher heat dissipation power (P_h) than Package **A**. It was explained to be due to the dielectric nature of ceramic which possible to eliminate the resistance caused by epoxy isolation layer.

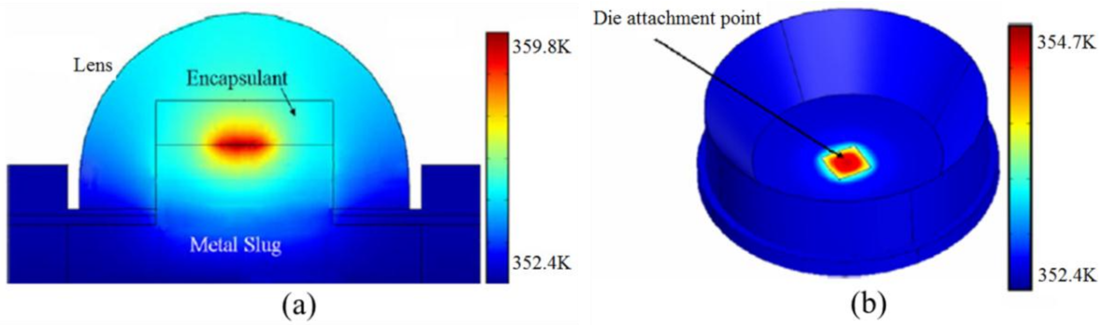

Figure 2.4: Simulation result of temperature distribution for: (a) Package **A** and (b) Package **B**. [Adapted from Christensen and Graham, 2007].

On the other hand, Yang, et al. (2007) suggested that the thermal performance of the ceramic package LED can be improved through thermal via. Different size and distribution of thermal via was punched onto ceramic sheet. The sample that was introduced as Type **I** consisted of single silver (Ag) thermal via with a diameter of 1.47mm and Type **II** consisted of 16 Ag thermal vias with a diameter of 0.43mm. Type **I** has the more contact area (A_c) between the chip and thermal via, but the less A_c between the thermal via and ceramic mold than Type **II**. The recorded thermal transient as demonstrated in Figure 2.5 showed that Type **II** performed weaker heat transfer due to the poor physical contact of the chip with thermal via. Modification has been made by increasing A_c of thermal via with the ceramic mold and introduced as Type **III**. The evaluated thermal transient and simulation result for Type **III** were shown in Figure 2.6.

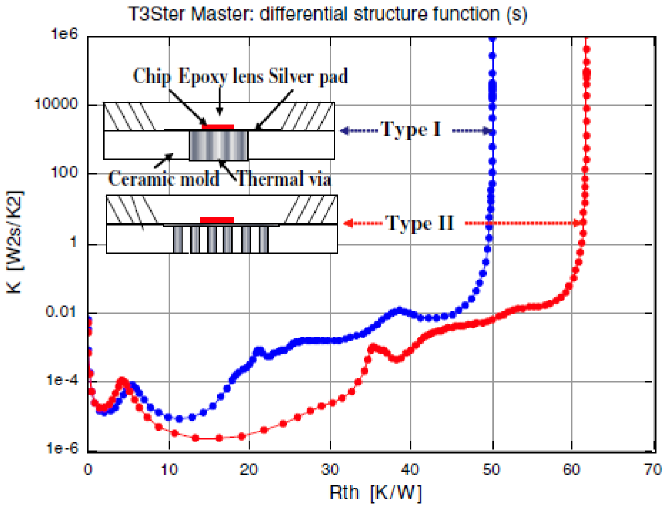

Figure 2.5: Thermal transients for Types **I** and **II**. [Adapted from Yang, et al., 2007].

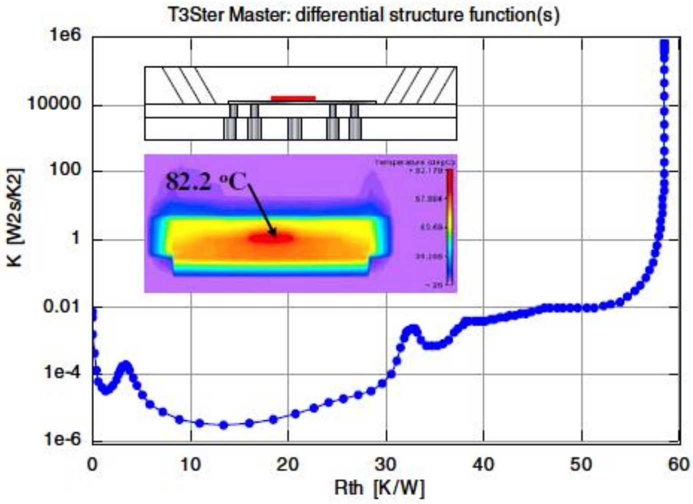

Figure 2.6: Thermal transient and simulation result for Type **III**. [Adapted from Yang, et al., 2007].

In this case, the finding showed that higher T_J was obtained. This indicated that A_c of thermal via with the chip has greater impact than with ceramic molds in the determination of thermal performance of the LED.

2.4 Modification on board-level and system-level

The improvement of the heat path in terms of package-level alone is insufficient to produce high end LED. Thus, researchers have moved forward and looked into the modification in terms of board-level and system-level of an LED package. Generally, board-level LED is composed by the mounting of a package-level LED on printed-circuit board (PCB) through the reflow soldering process. The application of PCB is able to provide the mechanical support to the package-level LED and the electrical connection. The most common selections of PCB are included FR-4 and metal-core board (MCB). The boards differ significantly in forms of the construction material properties. According to the product datasheet (*FR-4 glass/epoxy*, n.d.), FR-4 is a woven glass fabric with epoxy resin system which has lower *k* than the current approach as MCB. It was reported that MCB is a special form of circuit board with a dielectric layer bonded between a Cu conductive layer and metal substrate (Yung, 2007; *Led PCBs metal core PCBs (MCPCB)*, n.d.), as shown in Figure 2.7. Basically, MCB acts as a heat spreader by conducting the heat generated in a package-level LED effectively to ambient. The *k* of MCB can be improved by adding filler such as alumina (Al_2O_3) and boron nitride (BN) into the dielectric layer.

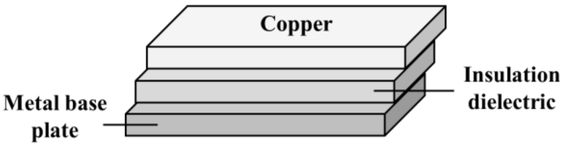

Figure 2.7: Schematic diagram of MCB. [Referred to Yung, et al., 2007].

On the other hand, the heat dissipation efficiency of a board-level LED can further be improved with the presence of an external heat sink by applying TIM between the interfaces, and introduced as system-level LED. However, it was reported that the orientation and design of a heat sink have brought to a greater impact on the thermal management of LED. In the earlier work as presented by Sparrow and Vemuri (1986), the orientation effect of pin-fin heat sink on the combined natural convection and radiation heat transfer has been studied. Findings demonstrated that the vertical up-facing fin yielded the highest *Q* than the sideward and vertical down-facing fins. The schematic diagram which illustrated the main flow for three of the different orientation pins was demonstrated in Figure 2.8.

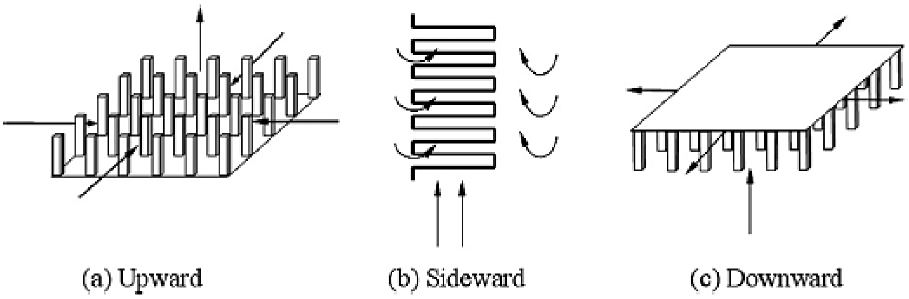

Figure 2.8: Schematic diagram of the main flow for the pins in orientations: (a) vertical up-facing, (b) sideward-facing and (c) vertical down-facing. [Adapted from Sparrow and Vemuri, 1986].

However, the enhancement of number of fins has led to the increased of heat transfer at first, after attaining a maximum, it reduced. Thus, the optimum amount of fin population as to obtain effective thermal management was defined. Moreover, Huang, et al. (2008) reported that Q was dependent on the finning factor and heat sink porosity. The finning factor represents the total surface area (A_T) divided by the base surface area (A_B); while heat sink porosity represents the volume fraction of fluid inside the heat sink.

In addition, Ekpu, et al. (2011) and Huang, et al. (2011) have carried out an investigation on the influence of heat sink geometry on thermal performance of LED. The schematic diagram of the heat sink geometry was shown in Figure 2.9.

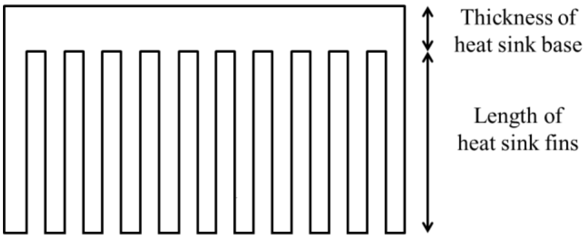

Figure 2.9: Schematic diagram of the heat sink geometry.

In the study, the thickness (t) of the heat sink base and the height of the heat sink fins were increased subsequently, while the chip size was kept constant. It showed that as the heat sink base thinner and heat sink fin extended to an optimum value, the better heat dissipation from an LED to ambient is allowed (Sahray, et al., 2010).

2.5 Die-attach and thermal interface material

Heat transfer fundamentals (n.d.) reported that the contact of two materials with imperfect surface may lead to the increase of thermal contact resistance. The formation of micro-air gaps or voids between the interfaces has reduced the heat conduction between the material layers, where air consists of low *k*. It was suggested that the use of TIM was useful in reducing the thermal contact resistance by eliminating the air-filled gaps. Figures 2.10(a) and 2.10(b) illustrate the interfaces of before and after the application of TIM, respectively. TIM available in various types such as phase change material, thermal tape, gap fillers and insulating pads have been developed for different applications.

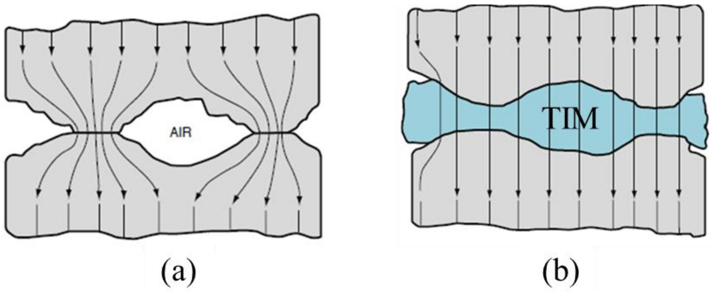

Figure 2.10: The interface of: (a) before and (b) after the application of thermal interface material. [Referred to *Heat transfer fundamentals*, n.d.].

Moreover, investigation on the quality of the die attach in high power LED has been carried out by Kim, et al. (2008). In the study, the selected die-attach materials were included Ag paste, solder paste and gold/tin (Au/Sn) eutectic bonding. Both the thermal transient characterization and FEM simulation have been conducted to determine the die-attach performance in thermal management of the LED. It was observed that the lowest package R_{th} was obtained in terms of the utilization of Au/Sn eutectic bonding as die attach material.

Nevertheless, Schweitzer, et al. has proposed two methodologies by applying the TIMs as boundary conditions in determining junction-to-case thermal resistance (R_{thJC}) through thermal transient recording (Schweitzer, et al., 2011) and FEA simulation (Schweitzer, 2008). The high repeatability and accuracy dual interface method has been accepted as JEDEC (Joint Electron Engineering Council) Standard JESD51-14 (*JEDEC Standard: JESD51-14 transient dual interface test method for the measurement of the thermal resistance junction to case of semiconductor devices with heat flow through a single path*, 2010). In this work, two sets of samples were adopted, where thermal grease or oil has been selected to be applied between a device and cold-plate, while the other without the use of any TIM. Figure 2.11 shows the recorded thermal impedance (*Zth*) in a function of time for both the conditions.

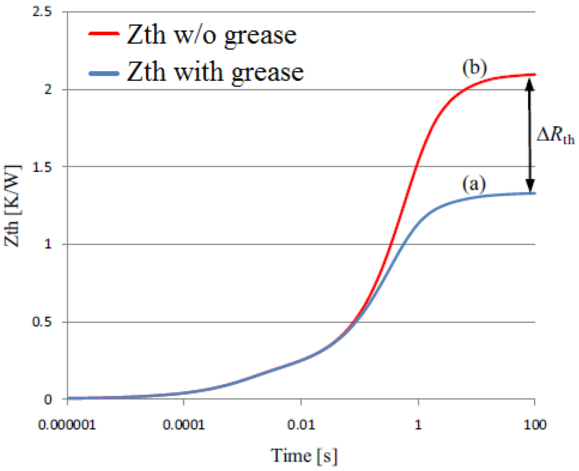

Figure 2.11: Thermal impedance in a function of time: (a) with and (b) without thermal grease. [Adapted from Schweitzer, et al., 2011].

It can be observed that there was an existence of the separation point in the functions during the comparison of with and without the presence of TIM (Szabo, 2005; Anithambigai, 2011). This indicated that the heat transferred from the device junction reaching to the interfaces between the end of device case and cold-plate, where R_{thJA} can be determined.

2.6 Improvement of thermal management

Forced convection is a mechanism where an external source such as pump, blower and fan is adopted to enhance the fluid motion of a heated surface and carry away the heat generated (*Forced convection heat transfer*, n.d.). The method of thermo-electric cooling (TEC) has been conducted by Li, et al. (2011) on high-power LEDs. The TEC effect was happening when I passed through the galvanic made by two different semiconductor materials in tandem mode, as shown in Figure 2.12. As I flow from n-type to p-type components, heat was absorbed and it became the cold end; in reverse, as I flow from p-type to n-type components, heat was released and it became the hot end (Bhushan, 2007; Lee, 2008; Saied, n.d.). In the study, the LEDs were attached to the cold end and the cooling fin was connected to the hot end. Thus, the heat generated from the LEDs was absorbed by the TEC and dissipated through the radiator.

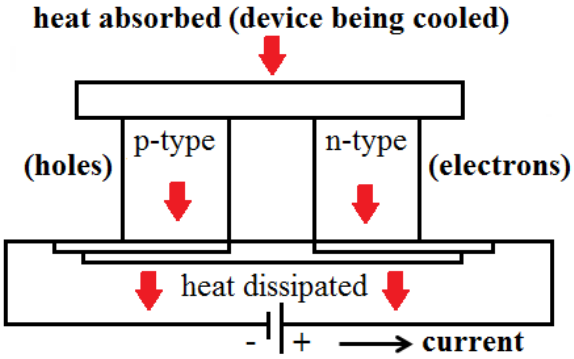

Figure 2.12: Mechanism of thermo-electric cooling. [Referred to Saied, n.d.].

Both T of the LED substrate and cooling fin were measured by using thermocouples. The obtained temperature variations (ΔT) of the LED substrate and cooling fins at 9W were demonstrated in Figure 2.13. It was observed that T of the LEDs was decreased rapidly at the beginning and increased softly until it achieved a stable state. But, T of the cooling fins was increased until it reached a steady state. With this, R_{thJA} of the LEDs system has been reduced under TEC. Besides, it was determined that the amount of heat absorbed and released was proportional to P_{in} of the TEC.

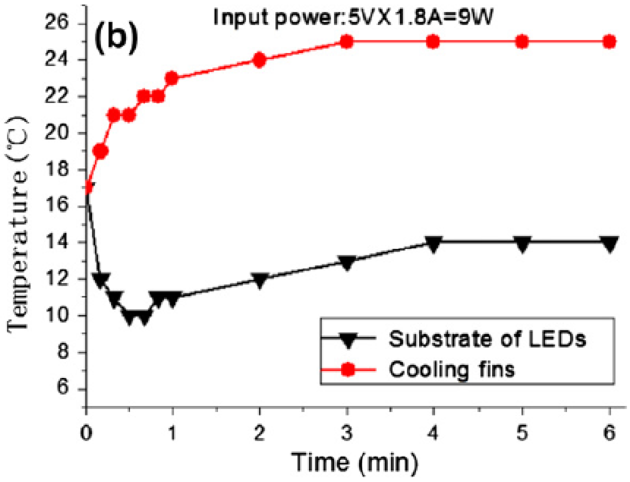

Figure 2.13: The temperature variations of the LED substrate and cooling fins at 9W. [Adapted from Li, et al., 2011].

Another forced convection method has been proposed by the researchers was the use of piezoelectric fans. Figure 2.14 shows the schematic diagram of piezoelectric fan. It was reported that the piezoelectric fan can be fabricated by bonding a thin metal or blade to piezoelectric element.

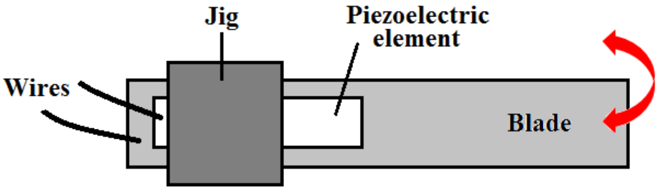

Figure 2.14: Schematic diagram of piezoelectric fan. [Adapted from Sauciuc, et al., 2010].

As the electrodes of the piezoelectric element were supplied with an alternating voltage (V), the occurrence of electric field will deform the element. Deformation of the element tended to expand and contract for the movement of the blade (Sauciuc, et al., 2010). It was studied by Acikalin, et al. (2004) that the fan frequency offset from resonance and the fan amplitude were the critical parameters in the enhancement of convective heat transfer. Since the low amplitude has caused slower air flow, the cooling capacity of the fan reduces correspondingly. In the designing of compact piezo fan cooling module as conducted by Tseng, et al. (2010) revealed that the vibration amplitude has been enhanced as V and resonant frequency increases. However, it was determined that there was an optimal resonant frequency of 60Hz in order to achieve the maximum vibration amplitude. In addition, the authors suggested that the slits on the blade can be set and inserted into the gaps between the heat sink fins to obtain a compact cooling module, as illustrated in Figure 2.15. Hence, the blade tips would have the similar resonance frequency and vibration amplitude.

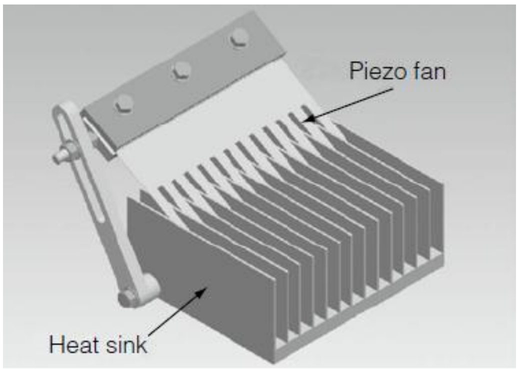

Figure 2.15: The compact cooling module. [Adapted from Tseng, et al., 2010].

On the other hand, Yoo, et al. (2000) has conducted a research to determine the relationship between different fan dimensions and materials with resonant frequency. The selected materials for fan were included phosphor bronze, brass and Al. The outcomes showed that the resonant frequency of the fan was dependent on its length, where higher frequency was obtained for shorter fan length. Moreover, the fan made of phosphor bronze has the highest fan tip displacement and fan velocity. Instead of the use of TEC cooling effect and piezoelectric fan, the application of the microjet cooling system has also been selected for thermal management of LED. Luo and Liu (2007) proposed a methodology on microjet array cooling system for high-power LEDs. The basic setup is shown in Figure 2.16.

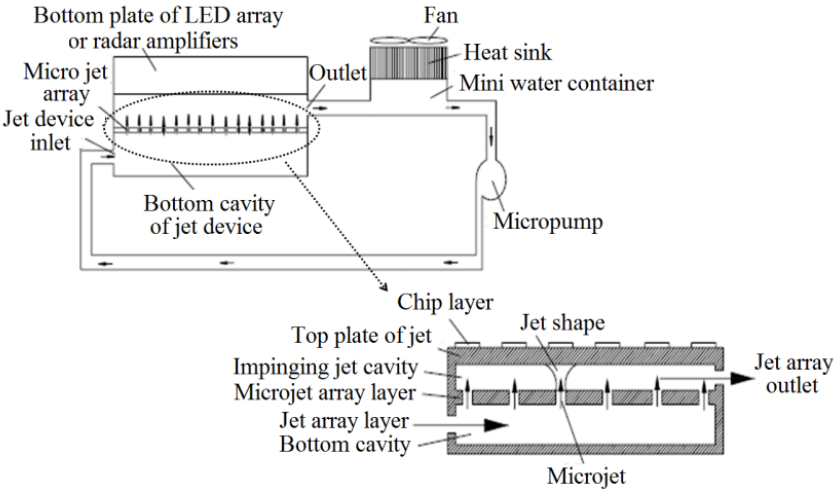
Bottom plate of LED array or radar amplifiers
Fan
Heat sink
Mini water container
Micro jet array
Outlet
Jet device inlet
Bottom cavity of jet device
Micropump
Chip layer
Jet shape
Top plate of jet
Impinging jet cavity
Microjet array layer
Jet array layer
Bottom cavity
Jet array outlet
Microjet

Figure 2.16: Basic setup of microjet cooling system for high power LEDs. [Adapted from Luo and Liu, 2007].

The work showed that the application of Cu as shell material has a significant effect in reducing the LED chip temperature than Al. Since the shell has a tight contact with the LED, Cu shell was capable to provide a better heat exchange between the heat dissipation from the LED and environment by natural convection through the shell surface. In addition, Liu, et al. (2006) demonstrated that with the application of the microjet cooling system, LED was able to work under high *I* at low operating *T*. In the other paper, Liu, et al. (2008) showed that the microjet with one inlet and two outlets was able to produce better heat transfer for an LED array.

2.7 Summary

The chapter has been compiled with the review on the works and outcomes as proposed by the researchers in the previous years. It can be seen that both the experimental and simulation characterizations have been carried out in order to investigate the LED properties precisely and accurately. Besides, different cooling methods and mechanisms have been suggested and applied as to enhance the heat dissipation capability of an LED. From the study, ideas and improvement in the thermal management of an LED were gained.

CHAPTER 3

METHODOLOGY AND INSTRUMENTATION

3.1 Overview

Generally, this chapter is divided into two main parts, which are the precise description on the proposed methodologies and the introduction on the characterization systems. In this work, thermal and optical characterizations are carried out on pre-molded and ceramic package LEDs under various measuring conditions. Initially, the samples preparations through reflow soldering process and basic poles connection are explained. This is followed by the calibration on the LEDs before the characterizations begin. There are in total six proposed methodologies. The procedure for the study on thermal and optical properties of the LEDs as I increased is presented in prior. Followed by the details on the process where the LEDs are attached to an external heat sink. Further investigations are performed on the selected LED package. The effect of TIM on thermal management of ceramic package LED is studied. Moreover, thermal performance of pre-molded package LED under the influence of different end surface convections and air-environments is studied. Later, the accuracy of thermal transient recording is determined through the study on the distinction between R_{thl} and R_{thr}. Lastly, the effect of various driving current modes for the LED operation is revealed.

3.2 Experimental works

3.2.1 Reflow soldering process and pole connection

Here, pre-molded and ceramic package LEDs mounted on MCB were used for investigations. An adequate amount of silicone-free solder paste CT-R00-30 with high *k* as 0.80 W/m·K that was formed by pre-blended of solder powder and flux (Rajewski, n.d.) was deposited between the package-level LED and MCB with designing pad. The excessive amount of solder paste will cause electrical short during the melting and reflow soldering process (Lee, 2002). Later, a package-level LED was picked up and placed slowly on it. It was cautioned that the pick and place actions should be carried out with a suitable tool by holding the housing without damaging the silicone lens of the LED. Figures 3.1(a) and 3.1(b) show the schematic diagrams of pre-molded and ceramic package LEDs, respectively.

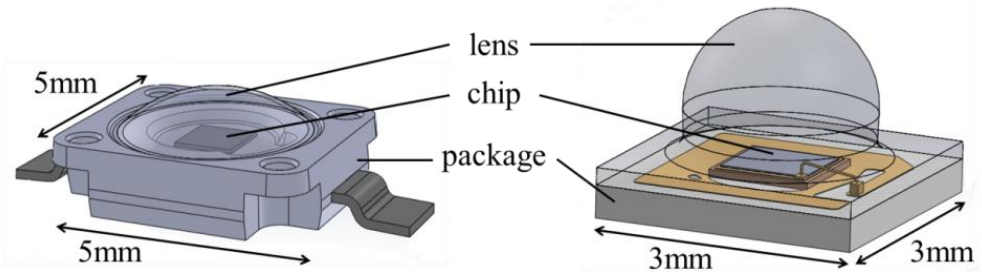

Figure 3.1: Schematic diagram of: (a) pre-molded and (b) ceramic package LEDs.

This was followed by reflow soldering which has been widely used for mounting process in surface mounting technology (SMT). In the process, the sample went through a well-controlled heating profile for duration of 300s. The temperature profile was set based on the potential impact on the LED to avoid harmful thermal stressing on it (Kirchner, et al., 2004). Figure 3.2 shows the reflow soldering profile for pre-molded and ceramic package LEDs.

During the heating, solder paste was melted and dispensed evenly onto the designed solder pad. Thus, the package-level LED was able to set well on top of it. The reflow soldering *T* was slowly decreased after the highest heating *T* was achieved. The gradual decrease of *T* was to produce solidification of solder paste (Henshall, et al., 2011). Finally, the sample was allowed to cool down to room temperature and ready for pole connection.

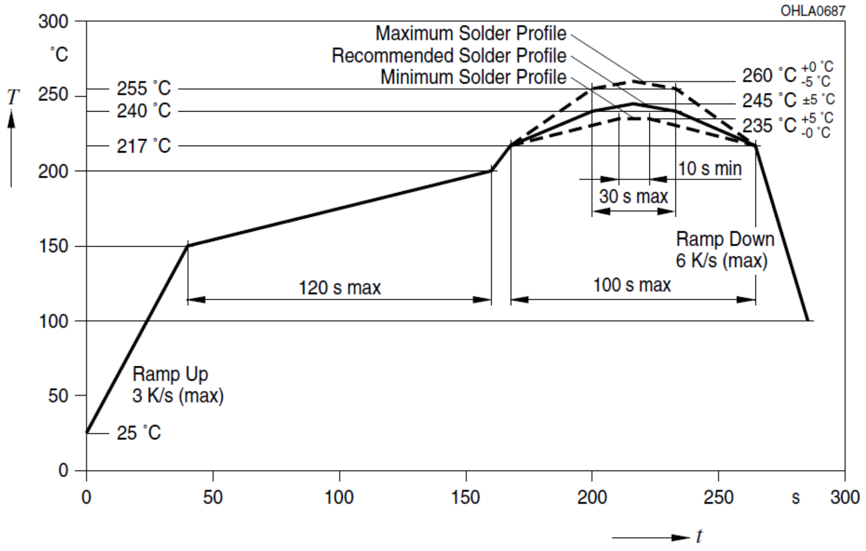

Figure 3.2: Reflow soldering profile for pre-molded and ceramic package LEDs.

Manual soldering was performed to connect the wire to the LED poles. In this case, both the lead-free solder wire and flux were utilized; while the red and black wires were used to indicate anode and cathode, respectively. The soldering iron was first heated to 250 ℃ in order to melt the solder wire. Meanwhile, the wire core was coated with a mild flux to produce strong solder joint. A thin layer of molten solder was touched onto the flux coated wire core and placed onto the contacts to complete the pole connection. Figure 3.3 demonstrates flowchart of the procedures for reflow soldering and pole connection.

3.2.2 LED calibration

Before thermal characterization begins, calibration process was performed on pre-molded and ceramic package LEDs to determine its Temperature-Sensitive Parameter (TSP) (Sofia, 1997; *JEDEC Standard: JESD51-1integrated circuits thermal measurement method – Electrical test method (single semiconductor device)*, 1995). TSP is defined as the ratio of ΔV to ΔT, as shown in equation 3.1.

$$TSP = \frac{\Delta V}{\Delta T} \tag{3.1}$$